Journal of Medicinal Chemistry



Article

# Carbon-11 and Fluorine-18 Radiolabeled Pyridopyrazinone Derivatives for PET Imaging of Phosphodiesterase-5 (PDE5)

Rufael Chekol, Olivier Gheysens, Muneer Ahamed, Jan Cleynhens, Peter Pokreisz, Greet Vanhoof, Stefan Janssens, Alfons Verbruggen, and Guy M Bormans

*J. Med. Chem.*, **Just Accepted Manuscript** • DOI: 10.1021/acs.jmedchem.6b01666 • Publication Date (Web): 06 Dec 2016



ACS Publications

Journal of Medicinal Chemistry is published by the American Chemical Society. 1155 Sixteenth Street N.W., Washington, DC 20036

# Carbon-11 and Fluorine-18 Radiolabeled Pyridopyrazinone Derivatives for PET Imaging of Phosphodiesterase-5 (PDE5)

*Rufael Chekol*[#,1] *Olivier Gheysens,*[2] *Muneer Ahamed,*[1] *Jan Cleynhens,*[1] *Peter Pokreisz,*[3] *Greet Vanhoof,*[4] *Stefan Janssens,*[3] *Alfons Verbruggen,*[1] *Guy Bormans*[1,*]

[1]KU Leuven, Department of Pharmaceutical and Pharmacological Sciences, Laboratory of Radiopharmacy, Leuven, Belgium

[2]KU Leuven, Department of Imaging and Pathology, Leuven, Belgium and Nuclear Medicine, UZ Leuven, Leuven Belgium

[3]KU Leuven, Department of Cardiovascular Sciences, UZ Leuven, Leuven, Belgium

[4]Discovery Sciences, Janssen Pharmaceutica, R&D, Beerse, Belgium

## Key words

cyclic guanosinemonophosphate (cGMP), phosphodiesterase 5 (PDE5), phosphodiesterase 5 inhibitors, pyridopyrazinones, PF-5, heart failure, pulmonary arterial hypertension, positron emission tomography (PET) tracers

## Abstract

The cyclic guanosine monophosphate (cGMP) specific phosphodiesterase type 5 (PDE5) plays an important role in various pathologies including pulmonary arterial hypertension and cardiomyopathy. PDE5 represents an important therapeutic and/or prognostic target but non-invasive assessment of PDE5 expression is lacking. The purpose of this study was to develop and evaluate pyridopyrazinone derivatives labeled with carbon-11 or fluorine-18 as PDE5-specific PET tracers. In biodistribution studies, highest PDE5-specific retention was observed for [$^{11}$C]-**12** and [$^{18}$F]-**17** in the lungs of wild-type mice and in the myocardium of transgenic mice with cardiomyocyte-specific PDE5 over-expression at 30 min post injection. In vivo dynamic microPET images in rats revealed that both tracers crossed the blood-brain barrier but brain retention was not PDE5-specific. Both [$^{11}$C]-**12** and [$^{18}$F]-**17** showed specific binding to PDE5 in myocardium of transgenic mice, however [$^{18}$F]-**17** showed significantly higher PDE5-specific inhibitable binding than [$^{11}$C]-**12**.


**Introduction** Phosphodiesterase type 5 (PDE5) is a member of the phosphodiesterase superfamily that specifically catalyzes and metabolically inactivates the second messenger cyclic guanosine monophosphate (cGMP). Under physiological conditions, PDE5 is expressed in vascular smooth muscle cells, lungs, platelets, corpus cavernosum and Purkinje fibers in the cerebellum, while expression in cardiomyocytes is minimal.[1-3] PDE5 exerts potent effects on vascular tone in the corpus cavernosum and pulmonary vasculature and plays an important role in platelet aggregation, handling of sodium secretion in renal cells and apoptosis.[2-4] PDE5 is also implicated in a number of diseases including pulmonary arterial hypertension (PAH) and ischemic and dilated cardiomyopathy.[3-9] The role of PDE5 in brain is still a subject of debate;

nonetheless, there is a general consensus that PDE5 is expressed in the cerebellum and in the hippocampal interneurons (in a scattered manner) of rodents.[10] The cGMP-PDE5 signaling pathway in rodent brain is considered to play a role in early memory consolidation stages of object information, neuronal excitability, synaptic plasticity and neurogenesis.[10-12]

Currently, several PDE5 inhibitors (sildenafil, vardenafil, tadalafil, and avanafil) have been approved for treating male erectile dysfunction and some of them (e.g.; sildenafil) are approved for treatment of PAH.[13-15] A number of authors also advocate the use of PDE5 inhibitors in cardiovascular diseases including heart failure and myocardial infarction since up-regulation of PDE5 in the myocardium has been observed in these conditions.[6,7,16-21] In addition, PDE5 inhibitors have also been shown to improve early memory consolidation of object information in rodents and functional recovery after stroke in rats.[22,23] However, it remains to be determined whether the distribution and physiological role of PDE5 in human brain is similar to that observed in rodents. Based on preclinical evidence, there might be a role for PDE5 inhibitors to improve functional recovery after stroke in patients but further investigation is warranted.

Despite the changes of PDE5 expression and/or activity under pathophysiological conditions and the success of PDE5 inhibitors in clinical practice, there is currently no method to non-invasively evaluate PDE5 expression and occupancy levels in vivo. The availability of PDE5-specific PET radioligands would allow (i) to quantify and evaluate spatiotemporal changes in PDE5 expression during disease progression, (ii) early identification of patients that would benefit from therapy with PDE5 inhibitors, (iii) and assessment of PDE5 occupancy and optimization of dose regimens in patients treated with PDE5 inhibitors.

In recent years, several attempts have been made to develop radioligands targeting PDEs with variable success.[24] Jacobsen et al. described the development of a PET radioligand, [$^{11}$C]RAL-01, for *in vivo* visualization of PDE5 although PDE5-specific binding could not be demonstrated.[25]

Our group published radiosynthesis and preliminary biological evaluation of a number of radiolabeled tracers targeting PDE5.[26] In that study, [$^{11}$C]-**7** ([$^{11}$C]NMVardenafil) was shown to be a selective and specific radiotracer with 87 % inhibitable PDE5 binding in the lungs of NMRI mice. However, none of the tracers were found to have any significant uptake in brain.

Here, we discuss the synthesis, radiolabeling and preliminary biological evaluation of derivatives of a novel brain penetrant PDE5 inhibitor reported in the literature, 3-(4-(2-hydroxyethyl)piperazin-1-yl)-7-(6-methoxypyridin-3-yl)-1-(2-propoxyethyl)pyrido[3,4-b]pyrazin-2(1H)-one (**PF-5**) [27], as potential radioligands for in vivo visualization of PDE5 (figure 1).

## Results and discussion

**Chemistry**. **PF-5** (**14**)**,** and compounds **10** and **18** (figure 1) were reported by Hughes et al. as selective and brain penetrant PDE5 inhibitors.[27] Compounds **12** (scheme 1a and 1b) and **17** (scheme 1c) are close analogues of **14** in which the 2-hydroxyethyl substituent on the piperazine ring of **14** was replaced by a methyl and 2-fluoroethyl substituent, respectively. We evaluated radiolabeled **12** and **17** as potential PET radioligands for in vivo visualization of PDE5.

Compound **6** was prepared from commercially available 6-chloro-3-pyridinamine as per reported literature (scheme 1a).[27] Treatment of the dione (**6**) with thionyl chloride in DMF at reflux temperature for 16 h yielded the chloroimidate intermediate **7** (59 % yield).[28] Reaction of **7** with *tert*-butyl piperazine-1-carboxylate or 2-(piperazin-1-yl)ethanol followed by standard Suzuki coupling with 6-methoxypyridin-3-ylboronic acid resulted in **9** (scheme 1b) and **14** (scheme 1c), respectively, with good overall yield. Standard deprotection of **9** with TFA and tosylation of **14** with tosyl chloride in the presence of triethylamine and trimethylammonium chloride[29] furnished precursors **10** and **15** for radiolabeling with carbon-11 and fluorine-18, respectively. The standard

non-radioactive references **12** and **17** were prepared by reacting the chloroimidate (**7**) with 1-methylpiperazine or 1-(2-fluoroethyl)piperazine followed by Suzuki coupling with 6-methoxypyridin-3-ylboronic acid. A detailed description of the synthesis of all compounds, $^{1}$H-NMR and HRMS data for intermediates, precursors and non-radioactive standard reference compounds is provided in supporting information.

**In vitro PDE5 inhibitory activity assay.** In vitro PDE5 inhibitory activity ($IC_{50}$) was determined for **10**, **12**, **14** and **17**. Their $IC_{50}$ values for selected families of phosphodiesterases (PDE5, PDE6 and PDE11) are given in table 1 ($IC_{50}$ values for 10 and 12 for PDE families are given in supporting information-table 1). The main purpose of the in vitro assay was to investigate the potential impact of the structural modification of **14** to allow radiolabeling with carbon-11 (compound **12**) or fluorine-18 (compound **17**). A major increase in the PDE5 $IC_{50}$ values for compounds **12** or **17** compared to compound **14** would invalidate the suitability of **12** and **17** as a PDE5 PET tracer. The selectivity results obtained in the in vitro assay for **12** indicate the radiotracer's specificity; high specificity is a prerequisite to avoid off target binding to other PDEs.

$IC_{50}$ values are dependent on assay conditions used, therefore only $IC_{50}$ values obtained under identical assay conditions should be compared. In our in vitro assay, the substrate (cGMP) concentration was 1 μM; whereas it was 50 nM in the assay used by Hughes et al[27]. This lower substrate concentration results in lower $IC_{50}$ values in comparison to the results we obtained.

The pyridopyrazinone derivatives (**10**, **14** and **18**) were reported to have an in vitro PDE5 inhibitory activity ($IC_{50}$) of respectively 3.28, 0.2, and 0.22 nM[27] showing a higher potency of compound **14** (2-hydroxyethyl-piperazine) and **18** (ethyl-piperazine) versus compound **10** (unsubstituted piperazine). In our assay the $IC_{50}$ values for **10** and **14** are five to tenfold higher than those reported by Hughes but in our conditions **14** was also found to be about tenfold more

potent than **10**. The $IC_{50}$ values of **12** (methyl-piperazine), and **17** (2-fluoroethyl-piperazine) were comparable and are intermediate between those of **10** and **14.** The results show that the structural changes (respectively methyl and 2-fluoroethyl instead of a hydroxyethyl substituent) required to allow radiolabeling, didn't result in drastic changes of $IC_{50}$ values. The selectivity of **12** against other PDEs in the in vitro assay was at least 300-fold whereas that of **14** was only 8-fold due to high affinity inhibition of hPDE1B1 (supporting information-table 1).

**Radiosynthesis.** Radiolabeling with carbon-11 was achieved by one-step N-alkylation of 0.5 mg of the amine precursor (**10**) in anhydrous DMSO with [$^{11}$C]methyl trifluoromethanesulfonate ([$^{11}$C]$CH_3OTf$) in the presence of base ($Cs_2CO_3$) at 90 °C for 2 min (scheme 2). Radiolabeling with fluorine-18 was achieved by [$^{18}$F]$F^-$ substitution for tosylate on **15** (0.5 mg in DMSO, scheme 2) at 90 °C for 15 min. The crude reaction mixtures were purified by RP-HPLC. The overall radiosynthesis, HPLC purification, sterile filtration and radiotracer formulation were completed in 50 to 90 min from end of bombardment.

The radiochemical yield, (RCY) based on HPLC analysis of the reaction mixture was 20 % and 31 % for [$^{11}$C]-**12** and [$^{18}$F]-**17**, respectively and the radiochemical purity after HPLC-purification was greater than 99 % for both compounds (table 2 and supporting information-table 2).

The identity of the labeled compounds was confirmed by co-injecting the corresponding non-radioactive reference compounds (**12** and **17**) on HPLC. The specific activities were determined after HPLC purification and were 67 GBq/μmol for [$^{11}$C]-**12** and 91 GBq/μmol for [$^{18}$F]-**17** (table 2) at the end of synthesis.

**Biological evaluation.** Pyridopyrazinone derivatives [$^{11}$C]-**12** and [$^{18}$F]-**17** were initially evaluated by assessing their uptake and retention in the lungs of mice because abundant physiologic expression of PDE5 in the lung tissue among different species has been reported by several authors.[2,13,15,30,31] Both tracers were also evaluated in transgenic mice with

cardiomyocyte-specific PDE5 over-expression (PDE5 TG) in which a significant myocardial retention was expected. The binding specificity of [$^{11}$C]-**12** and [$^{18}$F]-**17** to PDE5 both in lungs of wild-type mice and myocardium of PDE5 TG mice was challenged by pre-treating mice with tadalafil (a structurally unrelated competitive PDE5 inhibitor)[32] prior to intravenous (iv) radioactive tracer administration. Results of biodistribution experiments were expressed as percentage of injected dose (% ID) and as standardized uptake values based on weight ($SUV_W$, obtained by normalizing the % ID for the animal's body weight and the weight of organ of interest).

**Control wild-type mice (NMRI mice).** Although we performed biodistribution studies in the wild-type mice at 2, 10 and 30 min post injection (p.i.) for [$^{11}$C]-**12** and additionally 60 min for [$^{18}$F]-**17** the focus was put on the 30 min pi timepoint.

At 2 min p.i. both [$^{11}$C]-**12** and [$^{18}$F]-**17** were distributed to the major organs (kidneys, liver, lungs and intestines). The percentage injected dose of radioactivity in urine was low at all studied time points despite relatively high kidney retention and excretion occurred mainly via the hepatobiliary route (supporting information-tables 3 and 4).

The relative concentration (expressed as $SUV_w$) of [$^{11}$C]-**12** and [$^{18}$F]-**17** was the highest in the lungs of NMRI mice at all studied time points (supporting information-table 4). However, the clearance of [$^{11}$C]-**12** and [$^{18}$F]-**17** from the lungs was rapid as evidenced from retention of both tracers in lungs at 30 min p.i. was only 25% ([$^{11}$C]-**12**) and 19% ([$^{18}$F]-**17**) of the initial lung retention at 2 min p.i. We observed a slower lung clearance with a vardenafil derivative ([$^{11}$C]-**7**[26]**)** that we reported earlier. This vardenafil derivative had an $IC_{50}$ value of 0.8 nM and showed that activity in the lungs at 30 min p.i. was 70 % of that at 2 min p.i. This difference may be

explained by faster PDE5 dissociation kinetics of the pyridopyrazinone tracers compared to the vardenafil derivative.

The relatively high % ID radioactivity in blood for [$^{18}$F]-**17** compared to [$^{11}$C]-**12** both in control and PDE5 TG mice (figure 3) could be due to the large fraction of circulating radioactive metabolites.

Myocardial uptake and retention of both tracers in NMRI mice were negligible, which is concordant with known low expression levels of PDE5 in healthy myocardium. Interestingly, in contrast to most radiolabeled PDE5 tracers we have evaluated so far a relatively high brain uptake was observed for both [$^{11}$C]-**12** and [$^{18}$F]-**17** in agreement with the reported brain penetrant ability of **14**. Retention of [$^{11}$C]-**12** in the cerebrum and cerebellum was higher than that of [$^{18}$F]-**17** at all studied time points (4.0±0.9 and 1.5±0.1 % ID at 2 and 30 min p.i. for [$^{11}$C]-**12** and 2.4±0.3 and 1.2±0.1 % ID at 2 and 30 min p.i. for [$^{18}$F]-**17**, respectively, supporting information-table 3).

Treatment of male erectile dysfunction is the major clinical application of PDE5 inhibitors where they are used to inhibit cGMP degradation and maintain penile tumescence. Despite this fact, the maximum observed $SUV_W$ in the penis for both tracers was relatively low ($SUV_W < 0.9$, supporting information-table 4) which was expected in light of the lower expression of PDE5 in the corpus cavernosum compared to lung tissue.[30,31]

**Biodistribution in transgenic mice with cardiomyocyte-specific PDE5 over-expression (PDE5 TG).** The PDE5 TG mice are characterized by an up to 10-fold increase in cardiomyocyte-specific PDE5 protein expression and a 10-fold increase in sildenafil-inhibitable cGMP hydrolysis compared to wild type littermates.[6,7] These mice were used as a positive control

in the biodistribution studies of [$^{11}$C]-**12** and [$^{18}$F]-**17** at 30 min p.i. in order to further address the sensitivity and specificity of the radioactive tracers for PDE5.

Myocardial uptake in PDE5 TG mice was 10-fold and 16-fold higher (% ID) for [$^{11}$C]-**12** and [$^{18}$F]-**17**, respectively, compared to that in control mice (figures 2 and 3). Despite lower lung retention of [$^{18}$F]-**17** than that of [$^{11}$C]-**12** in control mice, its uptake in the myocardium of PDE5 TG mice was three-fold higher ($SUV_W$) than that of [$^{11}$C]-**12** at 30 min p.i. In contrast, $SUV_W$ values in lung tissue of PDE5 TG mice for [$^{11}$C]-**12** and [$^{18}$F]-**17** were almost 50 % ($p < 0.05$) and 24 % ($p = 0.09$) respectively, lower than that of the control mice. Although it is difficult to experimentally prove, we hypothesize that the reduced lung uptake is due to the ‘‘stealing effect’’ of the high myocardial uptake resulting in a reduced availability of circulating tracer. In contrast to the stronger PDE5 related lung retention, the myocardial retention of vardenafil derivative ([$^{11}$C]-**7**[26]) in TG mice was slightly lower than that of [$^{18}$F]-**17** at 30 min p.i. (8.2±0.6 for [$^{18}$]-**17** vs. 6.1±1.1 for the vardenafil derivative) (Chekol et al unpublished result). The difference between lung and myocardium may be due to species differences as mouse PDE5 is expressed in the lungs whereas bovine PDE5 is overexpressed in myocardium of transgenic mice.

**Blocking study in wild-type and PDE5 TG mice.** The PDE5-specific binding of [$^{11}$C]-**12** and [$^{18}$F]-**17** in the lungs of NMRI mice (N = 4) and myocardium of PDE5 TG mice (N = 4) was assessed by a pre-blocking biodistribution study in which mice were pre-treated with tadalafil 10 mg/kg, sc, 60 min prior to radiotracer administration.

Pre-treatment of NMRI mice with tadalafil resulted in significant reduction 32 % ($p < 0.05$) and 70 % ($p < 0.001$)) in lung retention of [$^{11}$C]-**12** and [$^{18}$F]-**17** based on % ID at 30 min p.i., respectively (supporting information-table 3 and 5).

Retention in the myocardium of PDE5 TG mice was markedly lower after tadalafil pre-treatment, with a reduction of 80 % ($p < 0.001$) for [$^{11}$C]-**12** and 87 % ($p < 0.0001$) for [$^{18}$F]-**17** compared to non-treated PDE5 TG mice based on % ID (supporting information-table 5). The reduction in retention of the radioactive tracers in the lungs of tadalafil pre-treated PDE5 TG mice was 19 % for [$^{11}$C]-**12** and 30 % for [$^{18}$F]-**17**, respectively, when compared to non-treated PDE5 TG mice but this difference was not statistically significant, (supporting information-table 5).

Pre-treatment with tadalafil did not result in reduction of brain activity for both tracers which is not surprising since tadalafil is known to exhibit very limited uptake in brain.

The tadalafil blocking study confirms that myocardial retention of [$^{11}$C]-**12** and [$^{18}$F]-**17** in TG mice is PDE5-specific whereas lung retention is only partially due to PDE5 binding, especially for [$^{11}$C]-**12.**

**Plasma and brain radiometabolite analysis**. Plasma and brain extracts were analyzed with HPLC to quantify the fraction of radiometabolites of [$^{11}$C]-**12** and [$^{18}$F]-**17** at 2 and 30 min p.i. (tables 3 and 4). At 2 min p.i. more than 90 % and 68 % of the activity recovered in the plasma was in the form of [$^{11}$C]-**12** and [$^{18}$F]-**17** respectively. However, at 30 min p.i. only 30 % of the activity recovered in the plasma was in the form of intact [$^{11}$C]-**12**. Despite structural similarity between the two radiotracers, [$^{18}$F]-**17** showed more extensive metabolism with only 5 to 7 % of activity in the plasma in the form of intact radiotracer at 30 min p.i. Defluorination of [$^{18}$F]-**17** is not likely as none of the radioactive metabolites showed retention time corresponding to that of fluoride (F-18) and deflourination would also have been reflected in increased bone uptake which was not observed in microPET images of mice injected with [$^{18}$F]-**17** (figure 5).

Two radiometabolites of [$^{18}$F]-**17** were detected, the most abundant (98% of total radiometabolites) eluting with a retention time (rt) of 2.3 min and one radiometabolite eluting close (rt 11.2 min) to the intact tracer (rt 12.2 min). In view of the small mass amounts of injected

tracer it is difficult to identify the radiometabolites but Hughes et al[27] reported that in their microsomal stability assay the major metabolite of **14** was generated by loss of the n-propoxy group, which should also occur in case of **12** and **17**. As fast metabolism usually contributes to more rapid plasma clearance and higher signal/noise ratios, fast metabolism can be beneficial for a PET tracer if the radiometabolites do not show on and/or off-target binding.

Apparently, both polar radiometabolites detected in plasma did not cross the blood brain barrier to any significant level, as most of the activity in brain (> 90%) was still in the form of intact tracer at 30 min p.i. (supporting information-table 8).

As the SUVw of [$^{18}$F]-**17** in myocardium of PDE5 TG mice was three-fold higher than that of [$^{11}$C]-**12,** only **[$^{18}$F]-17** was investigated with in vivo microPET imaging.

Both tracers were further investigated for their uptake and specificity for PDE5 in brain.

**MicroPET imaging:** ***Myocardial uptake.*** In vivo tracer kinetics of [$^{18}$F]-**17** were evaluated in PDE5 TG mice. Reversible but specific binding of [$^{18}$F]-**17** to PDE5 was assessed in PDE5 TG mice by chasing and blocking experiments using the structurally unrelated PDE5 inhibitor tadalafil.[32]

The myocardium of PDE5 TG mice injected with [$^{18}$F]-**17** showed a high peak SUVv value (6.7) followed by a brief transient equilibrium between 2 and 10 min p.i. (figure 4). The high myocardial uptake of [$^{18}$F]-**17** (6.7±0.3 SUVv) derived from dynamic microPET imaging is in line with the high myocardial retention observed in the PDE5 TG biodistribution study at 30 min p.i. (8.2±0.6 % ID, supporting information-table 5).

In the chase mice group, myocardial activity of [$^{18}$F]-**17** decreased very rapidly after intravenous administration of tadalafil illustrating reversibility of PDE5 specific binding in myocardium (figures 4 and 5). The specific binding of [$^{18}$F]-**17** to PDE5 in myocardium was further confirmed

by complete abolishment of myocardial tracer uptake in the case of pre-treatment with tadalafil (figure 4).

**MicroPET imaging:** ***Brain uptake.*** Dynamic microPET imaging was also performed in Wistar rats to evaluate the kinetics and binding properties of [$^{11}$C]-**12** and [$^{18}$F]-**17** in brain (figure 6 and 7). MicroPET images showed that both tracers crossed the blood brain barrier (BBB) and were retained in the brain with a relatively uniform distribution confirming biodistribution data obtained in mice. PDE5 specificity of binding could not be demonstrated due to the unavailability of a structurally unrelated PDE5 inhibitor that crosses the BBB. However, a self-blocking study with cold **17** in rats showed no significant difference in brain retention of [$^{18}$F]-**17** between rats pre-treated with **17** and non-treated rats (figure7) suggesting that the observed retention in brain is due to a non-specific mechanism such as lysosomal trapping which may be possible as the compound contains a basic amine. The latter might also be supported by the fact that a high lung uptake with an important non-blockable fraction was observed with [$^{11}$C]-**12** and [$^{18}$F]-**17**.[33] In addition, very low expression levels of PDE5 in brain have been described in literature.[2,10,30]

**In vitro autoradiography.** Rat brain slices were used for in vitro autoradiography (figure 8) with [$^{11}$C]-**12** and [$^{18}$F]-**17** alone or in the presence of different competitive PDE5 inhibitors: 20 μM of either NMVardenafil (**7**)[26], tadalafil[32], **14**, or **12**, and 1 mM of 3-isobuty-1-methylxanthin/IBMX). IBMX is a non-selective phosphodiesterase inhibitor with an *in vitro* PDE inhibitory activity ($IC_{50}$) ranging from 2 μM to 50 μM.[34-37]

A uniform distribution throughout the grey matter was observed in slices incubated with either [$^{11}$C]-**12** or [$^{18}$F]-**17**. Moderate (27-45%) binding inhibition of [$^{11}$C]-**12** and [$^{18}$F]-**17** was observed in self-blocking conditions and blocking with **14**, but to a much lesser extent upon

blocking with IBMX or the PDE5 specific inhibitors 7 (NMVardenafil)[26] and tadalafil[32] (figure 8).

The results of the autoradiography experiments are in line with our hypothesis of lysosomal trapping of the studied tracers, which indeed may be partially blocked using high concentrations of pyridopyrazinone derivatives but not by IBMX, tadalafil and NMVardenafil. [$^{11}$C]-**12** and [$^{18}$F]-**17** both show high brain exposure but PDE5 expression levels may be too low to be detected especially in the presence of high background resulting from non-saturable binding.

The aim of this study was to evaluate two potential PET radioligands for imaging PDE5 in the lungs, myocardium and brain because 1) PDE5 inhibitors are approved for treating pulmonary hypertensions, 2) there is cumulative preclinical and clinical evidence that selective PDE5 inhibitors have beneficial effects on cardiac disease (e.g. ischemic and dilated cardiomyopathy) and 3) there is preclinical evidence that PDE5 is a therapeutic target for stroke and PDE5 in the brain represents an interesting target. The ability to differentiate those patients showing PDE5 over-expression from the normal expressing ones with radiolabeled PDE5 specific radioligands such as [$^{18}$F]-**17** may enable the physician to tailor the treatment regimen on individual basis. Also, study of PDE5 receptor occupancy with [$^{18}$F]-**17** may assist in the determination of dose and dosage regimens for individual patients.

The availability of PET tracers for in vivo visualization and quantification of PDE5 in the myocardium is paramount importance because PDE5 expression levels in the myocardium have been investigated by immunoblot and/or immunohistochemistry of explanted heart or on myocardial biopsies.[5-9] Our preliminary investigation of [$^{11}$C]-**12** and [$^{18}$F]-**17** in transgenic mice with over-expression of human PDE5 showed the potential of [$^{18}$F]-**17** for in vivo visualization and quantification of PDE5 expression in the myocardium of heart failure patients with positron

emission tomography and investigation of myocardial PDE5 occupancy levels after pharmacologic PDE5 inhibition .

The extent of PDE5 expression in brain (particularly in purkinje fibers) is still a topic of debate[10-12], our study confirms brain exposure of pyridopyrazinone based PDE5 inhibitors which can thus be used experimentally to inhibit brain PDE5, despite the fact that [$^{11}$C]-**12** and [$^{18}$F]-**17** are not useful to visualize PDE5 in brain due to high non-specific tracer retention in brain.

## Conclusion

We have successfully radiolabeled two close analogues of **PF-5,** a pyridopyrazinone derivative which was initially reported as a brain penetrant PDE5-specific inhibitor. In vivo specific binding to PDE5 was established in a transgenic mouse model with cardiomyocyte-specific over-expression of PDE5. The high myocardial uptake in PDE5 TG mice was blocked efficiently by pre-treatment with the structurally unrelated PDE5-specific inhibitor tadalafil. Although high brain uptake and retention was observed, this was found not to be PDE5-specific and is due to non-saturable binding (we hypothesize lysosomal trapping), as self-blocking in vivo did not result in any significant reduction in brain uptake. Our preliminary in vivo biological evaluation confirmed the high affinity and binding specificity of [$^{11}$C]-**12** and [$^{18}$F]-**17** to PDE5 with the latter compound showing significantly higher PDE5-specific inhibitable binding in lungs and myocardium of mice that over-express myocardial PDE5. [$^{18}$F]-**17** shows a similar uptake in myocardium of transgenic mice compared to a previously reported radiolabeled vardenafil derivative and comparative clinical studies will be required to evaluate which of both tracers is best suited for visualization of PDE5 in humans with PET. Our findings necessitate further experiments in clinically relevant animal models and/or patients with cardiovascular pathology with altered PDE5 expression to evaluate the suitability of these radiotracers in the clinic.

## Experimental section

**Chemistry.** $^1$H-NMR spectra were recorded on a 400 MHz spectrometer (Bruker AVANCE) and either, deuterated chloroform ($CDCl_3$) or deuterated methanol (MeOD) or deuterated dimethyl sufoxide (DMSO-$d_6$) was used as a solvent as indicated. Chemical shifts are reported in parts per million relative to tetramethylsilane ($\delta = 0$). Coupling constants are reported in hertz (Hz). Splitting patterns are defined as follow: s (singlet), brs (broad singlet), d (doublet), q (quartet), dd (double doublet), t (triplet), dt (double triplet), or m (multiplet).

High-performance liquid chromatography (HPLC) analysis was performed on a LaChrom Elite HPLC system (Hitachi) connected to a UV-spectrometer set at 254 nm. For the analysis of radiolabeled compounds, the HPLC eluate (after passage through the UV detector) was led over a 7.62-cm (3-in.) NaI(Tl) scintillation detector connected to a single-channel analyzer (GABI box; Raytest, Straubenhard, Germany). Quantification of radioactivity measurements in biodistribution studies was performed using an automated $\gamma$-counter equipped with a 7.62-cm (3-in.) NaI(Tl) well crystal coupled to a multichannel analyzer (1480 Wizard; Wallac, Turku, Finland). The results were corrected for background radiation and decay during counting.

All solvents and chemicals were obtained from commercial sources (Acros Organics, Aldrich or Fluka unless specified otherwise) and used as such without further purification. Purity of all final compounds (precursors and references) was ≥ 95 % and was determined by HPLC.

Intermediates, precursors and non-radioactive standard references were characterized by, LC-HRMS and $^1$H-NMR.

A detailed description of the synthesis of all compounds with their $^{1}$H-NMR and HRMS data is provided in the supporting information.

**In vitro affinity assay.** Compounds **10**, **12**, **14** and **17** were dissolved in DMSO to a concentration of 5 mM. These compounds were profiled on the PDE assay platform, comprising members of each of the 11 described PDE families. PDE1B1 and PDE11A4 were expressed in human embryonic kidney (HEK) cells from full-length human recombinant clones. Human recombinant phosphodiesterases 2A, 4D3, 5A3, 7A1, 9A1, 10A2 were expressed in Sf9 cells, using a recombinant baculovirus construct containing the full-length sequence with a 6×His sequence following the start Met to allow metal affinity purification of the recombinant protein. Cells were harvested and the phosphodiesterase protein was purified by metal chelate chromatography on Ni-sepharose 6FF (GE Healthcare, Amersham Biosciences AB, Björkgatan 30, 751 84 Uppsala, Sweden). PDE3B, PDE6AB and PDE8A were purchased as partially purified Sf9 cell lysates (Scottish Biomedical, Glasgow, UK). All enzymes were dissolved in a mixture containing 50 mM Tris pH 7.8, 1.7 mM EGTA and 8.3 mM $MgCl_2$, except for PDE9A that was diluted in a mixture of 50 mM Tris pH 7.8 and 5 mM $MnCl_2$. PDE1B was dissolved in a mixture of 50 mM Tris pH 7.8, 1.7 mM EGTA and 8.3 mM $MgCl_2$ complemented with 624 U/mL calmodulin and 800 μM $CaCl_2$. The affinity of the compounds for the PDEs was measured by a scintillation proximity assay (SPA).

PDE yttrium silicate SPA beads (Amersham Biosciences Amersham Place Little Chalfont Buckinghamshire England HP7 9NA) allow PDE activity to be measured by direct binding of the primary phosphate groups of non-cyclic AMP or GMP to the beads via a complex iron chelation mechanism. The amount of bound tritiated product ([$^{3}$H]-AMP or [$^{3}$H]-GMP) was measured by liquid scintillation counting in a TopCount instrument (Perkin Elmer).

The compounds were dissolved in DMSO in polystyrene plates to a concentration of 100-fold the final concentration in the assay. Human recombinant PDE5A3 enzyme solution (10 µL) was added to 20 µL of incubation buffer (50 mM Tris pH 7.8, 8.3 mM $MgCl_2$, 1.7 mM EGTA), 10 µL substrate solution consisting of a mixture of non-tritiated and tritiated substrate (final concentration 1 µM cGMP, 370 Bq $^3$H-cGMP), and 0.4 µL compound in DMSO in a 384-well plate, and the mixture was incubated for 30 minutes at room temperature. After incubation, the reaction was stopped with 20 µL of stop solution, consisting of PDE SPA beads (17.8 mg beads/mL in 200 mM zinc chloride). To measure the blank value, the enzyme was omitted from the reaction mixture. After sedimentation of the beads for 30 minutes, the radioactivity was measured in a PerkinElmer TopCount scintillation counter and results were expressed as counts per minute (cpm). The same assay principle was applied for the measurement of the inhibition of other members of the PDE family, with appropriate modifications of enzyme concentration, incubation buffer, substrate solution, incubation time and stop solution. Each experiment was performed in duplicate.

Data were calculated as the percentage of inhibition of total activity measured in the absence of test compound (% control). A best-fit curve is fitted by a minimum sum of squares method to the plot of percent control versus compound concentration, from which an $IC_{50}$ value (inhibitory concentration causing 50 % inhibition of hydrolysis) is obtained.

**Radiosynthesis.** Carbon-11 was produced in a Cyclone 18/9 cyclotron (IBA, Louvain-la-Neuve, Belgium) via an $^{14}N(p,\alpha)^{11}C$ nuclear reaction. A mixture of $N_2$ (95 %) with $H_2$ (5 %) was irradiated with 18-MeV protons for 30 minutes to get [$^{11}$C]methane ([$^{11}$C]$CH_4$). [$^{11}$C]$CH_4$ was transferred to a home-built synthesis module to convert it into [$^{11}$C]$CH_3I$ which was then converted to the more reactive [$^{11}$C]methyl triflate ([$^{11}$C]$CH_3OTf$) by passing through a silver triflate column (150 mm × 3 mm) heated at 180 $^{o}$C.

$[^{11}C]CH_3OTf$ was streamed with helium through a solution of 250 - 500 μg precursor in DMSO. The reaction mixture was heated at 90 °C for 2 min, cooled and diluted with buffer. The crude reaction mixture was purified by HPLC (XBridge C18 column, 5μm, 4.6 mm × 150 mm; Waters) using a mixture of 0.05 M sodium acetate pH 5.5 and ethanol, 63:37 % v/v at a flow rate of 1 mL/min as the mobile phase. The peak of interest was collected and analyzed for purity and identity before biological evaluation. For evaluation of the tracers in animals, the ethanol in the HPLC eluate was diluted with normal saline to a maximum concentration of 10 % ethanol and then sterile filtered through a 0.22-μm membrane filter (Millipore Millex GV 13 mm). Chemical and radiochemical purity of tracers were assayed with HPLC (XTerra C18 column, 5 μm, 4.6 mm × 100 mm, Waters) eluted with a mixture of acetate buffer (0.05 M, pH 5.5) and acetonitrile (ACN), 70:30 v/v at a flow rate of 1 mL/min, UV detection at 254 nm.

$[^{18}F]$Fluoride ($^{18}F^-$) was produced in a Cyclone 18/9 cyclotron (IBA) via an $^{18}O(p,n)^{18}F$ nuclear reaction by bombarding oxygen-18 enriched water ($H_2{}^{18}O$) with 18-MeV protons. $[^{18}F]F^-$ was then passed through a preconditioned (by successive washing with 10 mL of 0.5 M $K_2CO_3$ solution and 10 mL of de-ionized water) anion exchange cartridge (SepPak Light Accell plus QMA, Waters) to get rid of the bulk of the $H_2{}^{18}O$. $[^{18}F]F^-$ was then eluted with a mixture of 24 mM $K_2CO_3$/98 mM Kryptofix 2.2.2 (4,7,13,16,21,24-hexaoxa-1,10-diazabicyclo[8.8.8]-hexacosane) in 750 μL of a mixture of ACN:water (95:5 v/v) into a reaction vial. Any remaining water was removed by azeotropic distillation with ACN. An amount of 250 - 500 μg of the tosyl precursor in DMSO was added to the $[^{18}F]F^-$ containing vial and the mixture was heated at 90 $^oC$ for 15 min. The purification, formulation, sterile filtration, and quality control were done in similar conditions as for those carbon-11 labeled compounds.

**Biological evaluation.** All animal experiments were conducted according to the Belgian code of practice for the care and use of animals, after approval from the Animal Ethics Committee, KU Leuven (Ethische Commissie Dierproeven, KU Leuven, License number: LA1210237).

For biodistribution studies adult NMRI mice (N = 4 mice per time point) and/or transgenic mice with cardiomyocyte specific PDE5 over-expression (PDE5 TG, N = 4)[6], weighing 25 to 40 g, were used. Animals were housed in individually ventilated cages in a thermo-regulated (22 °C), humidity-controlled facility under a 12 h/12 h light/dark cycle, with free access to food and water.

Biodistribution studies of carbon-11 or fluorine-18 labeled tracers was performed in healthy NMRI mice at 2, 10, 30, and 60 min post injection (N = 4 mice/time point). The biodistribution study in PDE5 TG mice (N = 4) was performed at 30 min p.i. Mice were anesthetized with 2.5 % isoflurane in oxygen at a flow rate of 1 L/min and 7 MBq of [$^{11}$C]-**12** or 740 kBq of [$^{18}$F]-**17** was injected via a tail vein. The animals were sacrificed by decapitation at the specified time points. Blood and major organs were collected in tared tubes and weighed. The radioactivity in blood and organs was counted using an automated γ-counter and expressed as a percentage of injected dose (% ID) and standardized uptake value based on weight ($SUV_W$). For the calculation of total radioactivity in blood, muscle and bone, weight was assumed to be 7 % of body weight for blood, 12 % for bone and 40 % for muscle.

In order to assess the affinity and specificity of [$^{11}$C]-**12** and [$^{18}$F]-**17** for PDE5, a blocking study was performed in control and PDE5 TG mice. In brief, mice were subcutaneously (sc) injected with tadalafil (TCR, Toronto Research Chemicals, Brisbane Rd.,Toronto, Ontario, Canada) 10 mg/kg, 60 minutes prior to tracer administration. Tadalafil solution for injection was prepared in such a way that the final concentration was 1 mg/mL in 10 % dimethylsulfoxide in 40% (2-hydroxypropyl)-β-cyclodextrin solution and sterile filtered through a 0.22-μm filter (Millex-GV,

Millipore, Arklow, Ireland). Biodistribution study was then performed as described above and results were expressed as % ID and SUV.

**Radiometabolites analysis.** Radiometabolites of [$^{11}$C]-**12** and [$^{18}$F]-**17** in plasma of mice at 2 (N = 2) and 30 (N = 3) min p.i. were quantified. Mice were anesthetized with 2.5 % isoflurane in oxygen at a flow rate of 1 L/min and injected with 7.4 MBq [$^{11}$C]-**12** or [$^{18}$F]-**17** via a tail vein. The mice were decapitated at the desired time point, blood was collected into lithium heparin-containing tubes (4.5-mL lithium heparin PST tubes, BD Vacutainer; BD, Franklin Lakes, New Jersey) and stored on ice. After centrifugation (420 × g; 10 min) of blood, plasma was separated and analyzed by RP-HPLC on a Chromolith RP C18 column (3 mm×100 mm; Merck) eluted with gradient mixtures of $CH_3CN$ (A) and 0.05 M NaOAc pH 5.5 (B) (0-4 min: isocratic 0 % A, 0.5 mL/min; 4-9 min: linear gradient 0 % Λ to 90 % Λ, 1 mL/min; 9-12 min: isocratic 90 % A, 1 mL/min; 12-15 min: linear gradient 90 % A to 0 % A, 0.5 mL/min). The non-radioactive standard reference compound **12** or **17** was co-injected to identify the peak of the intact parent tracer. The eluate from the UV detector was passed through a 3-in. NaI(Tl) scintillation detector, connected to a single channel analyzer. The eluate from the radiodetector was collected as 1-mL fractions (Bio-Rad, Hercules, Canada). The radioactivity in each fraction was measured using an automated gamma counter.

Radiometabolites of [$^{11}$C]-**12** or [$^{18}$F]-**17** in brain of mice were quantified at 2 and 30 min after iv injection of the tracer (N = 2 per time point). Mice were sacrificed by decapitation at the desired time point. Brain was isolated and homogenized in acetonitrile. The crude mixture was filtered through a syringe filter (0.2-µm nylon Acrodisc 13, Acrodisc Syringe Filters, PALL Life Sciences Belgium, Hoegaarden). The filtrate was spiked with 5 µL of a 1 mg/mL solution of cold **12** or **17** and analyzed on HPLC (Xbridge RP C18 5 µm column, 4.6 mm×150 mm; UV

detection at 254 nM, eluted with a mixture of ACN and 0.05 M NaOAc pH 5.5, 32:68 v/v, at a flow rate of 1 mL/min).

**Small-Animal PET Studies.** Dynamic microPET imaging experiments were performed on a Focus 220 microPET scanner (Concorde Microsystems, Knoxville, Tenesse, USA). For all mice experiments, male PDE5 TG mice were used. During scanning, animals were kept under gas anesthesia (2.5 % isoflurane in $O_2$ at a flow rate of 1 L/min). Dynamic 90-min scans were acquired in list mode. Acquisition data were separated into 24 time frames (frame × time, 4 × 15 s, 4 × 60 s, 5 × 180 s, 8 × 300 s and 3 × 600 s) and reconstructed with maximum a posteriori (MAP) estimation. Time-activity-curves (TAC) were generated for the myocardial region for each individual scan, using PMOD software (version 3.1; PMOD Technologies, Zürich, Switzerland). The radioactivity concentration in the heart region was expressed as standardized uptake value based on volume ($SUV_V$) as a function of time after injection of the radiotracer by normalization of the local tracer concentration for body weight of the animal and injected dose. Baseline imaging, blocking and chase experiments were performed in PDE5 TG mice. Tadalafil was used for pre-treatment and chase. Mice were intravenously injected with 7 MBq of formulation of [$^{18}$F]-**17**. For blocking studies mice were pre-treated with 10 mg/kg tadalafil, subcutaneously, 60 minutes prior to tracer administration and for chase studies mice were given tadalafil 10 mg/kg, intravenously (intravenously, iv), 10 min after the start of PET acquisition. The solution of tadalafil, which is a specific PDE5 inhibitor with subnanomolar $IC_{50}$ value[32], was prepared in such a way that the final concentration was 1 mg/mL in 10 % dimethylsulfoxide in 40 % (2-hydroxypropyl)-β-cyclodextrin solution and the solution was sterile filtered via a 0.22-μm membrane filter. A baseline microPET imaging was also performed in two Wistar rats after iv injection of [$^{11}$C]-**12** or [$^{18}$F]-**17** to assess the tracers' distribution in the brain.

**In vitro autoradiography.** Rat brain slices of 20 µm thick serial sections mounted on slides were used for in vitro autoradiography studies. Brain slices were incubated with 400 µL of 370 kBq/mL solution of [$^{11}$C]-**12** or [$^{18}$F]-**17** alone (control), or in the presence of 1 mM IBMX, 20 µM tadalafil, 20 µM NMVardenafil[26], 20 µM **14**, 20 µM cold **12** or **17** for 30 minutes. Then, the slices were rinsed twice (2×5 min) with 50 mM Tris-HCl pH 7.4 containing 0.3 % BSA at 4 °C. After a quick dip in water at room temperature, the slices were dried.

Autoradiograms were obtained by exposing the slices for 30 min to a high-performance phosphor screen (Canberra Packard, Meriden, CT, USA). The images were analyzed with Optiquant software (Canberra Packard) and the radioactivity concentration in the autoradiograms was expressed in digital light units (DLU) per square millimeter.

**Statistics.** All calculated results are expressed as mean ± standard deviation (SD). For comparison, the Student's t-test was used and $p < 0.05$ was considered statistically significant.

## ASSOCIATED CONTENTS

**Supporting information:** Details of the synthesis of the studied compounds, NMR spectra, MS, and biodistribution data are available at http://pubs.acs.org.

## AUTHOR INFORMATION

***Corresponding author**: Prof. Guy Bormans, Address: O&N2, Herestraat 49, box 821, BE-3000 Leuven, Belgium; E-mail: guy.bormans@pharm.kuleuven.be; Phone: +32 16 330447; fax: +32 16 330449.

**#Present address:** Email: rufdaqua@yahoo.com, Medical Imaging, College of Medicine, University of Sasketchewan, Saskatoon, Canada.

**Author Contributions**

The manuscript was written through contributions of all authors.

**Funding sources.** We would like to express our appreciation for the financial support from In Vivo Molecular Imaging Research (IMIR) and Fonds Wetenschappelijk Onderzoek Vlaanderen (FWO). OG is holder of a senior clinical investigator mandate of the Fund for Scientific Research Flanders.

## ACKNOWLEDGMENT

We would like to thank Ann Van Santvoort, Julie Cornels, Jana Hemelaers and Ivan Sannen for their technical assistance during animal experiments.

## ABBREVIATIONS

% ID, Percentage of Injected Dose; BBB, Blood-Brain Barrier; CPM, Counts Per Minute; $IC_{50}$, Inhibitory Concentration at 50 %; ID, Injected Dose; kBq, kilobecquerel ($10^3$ Bq); MBq, Megabecquerel ($10^6$ Bq); NMRI, North Medical Research Institute; PAH, Pulmonary Arterial Hypertension; IV, intravenously; PDE5, Phosphodiesterase type 5; PDE5 TG, Phosphodiesterase type 5 TransGenic (transgenic mice with caradiomyocte specific over-expression of PDE5); PET, Positron Emission Tomography; p.i., Post Injection; RCY, RadioChemical Yield; SC, Subcutaneously; SUV, Standardized Uptake Value; TAC, Time-Activity-Curve.

## REFERENCES

(1) Lukowski, R.; Krieg, T.; Rybalkin, S.D.; Beavo, J.; Hofmann, F. Turning on cGMP-dependent pathways to treat cardiac dysfunctions: boom, bust, and beyond. *Trends Pharmacol. Sci.* **2014**, *35*, 404-413.

(2) Lin, C. S.; Lin, G.; Xin, Z. C.; Lue, T. F. Expression, distribution and regulation of phosphodiesterase 5. *Curr. Pharm. Des*. **2006**, *12*, 3439-3457.

(3) Tsai, E. J.; Kass, D. A. Cyclic GMP signaling in cardiovascular pathophysiology and therapeutics. *Pharmacol. Ther.* **2009**, *122*, 216-238.

(4) Kass, D. A.; Champion, H. C.; Beavo, J. A. Phosphodiesterase type 5 expanding roles in cardiovascular regulation. *Circ. Res.* **2007**, *101*, 1084-1095.

(5) Nagendran, J.; Archer, S. L.; Soliman, D.; Gurtu, V.; Moodily, R.; Haromy, A. Phosphodiesterase type 5 is highly expressed in the hypertrophied human right ventricle, and acute inhibition of phosphodiesterase type 5 improves contractility. *Circulation* **2007**, *116*, 238-248.

(6) Pokreisz, P.; Vandenwijngaert, S.; Bito, V.; Van den Bergh, A.; Lenaerts, I.; Busch, C.; Marsboom, G.; Gheysens, O.; Vermeersch, P.; Biesmans, L.; Liu, X.; Gillijns, H.; Pellens, M.; Van Lommel, A.; Buys, E.; Schoonjans, L.; Vanhaecke, J.; Verbeken, E.; Sipido, K.; Herijgers, P.; Block, K. D.; Janssens, S. P. Ventricular phosphodiesterase-5 expression is increased in patients with advanced heart failure and contributes to adverse ventricular remodeling after myocardial infarction in mice. *Circulation* **2009**, *119*, 408-416.

(7) Vandenwijngaert S.; Pokreisz P.; Hermans H.; Gillijns H.; Pellens M.; Bax A.; Coppiello G.; Oosterlinck W.; Balogh A.; Papp Z.; Bouten V.; Bartunek J.; D'hooge J.; Luttun A.; Verbeken E.; Herregods C.; Herijgers P.; Bloch D.; Janssens S. Increased cardiac myocyte PDE5 levels in human and murine pressure overload hypertrophy contribute to adverse LV remodeling. *PLoS One* **2013**, *8*,e58841.

(8) Lu, Z.; Xu, X.; Hu, X.; Lee, S.; Traverse, J. H.; Zhu, G.; Fassett, J.; Tao, Y.; Zhang, P.; dos Remedios, C.; Pritzker, M.; Hall, J. L.; Garry, D. J. Chen, Y. Oxidative stress regulates left ventricular PDE5 expression in the Failing Heart. *Circulation* **2010**, *121*, 1474-1483.

(9) Shan, X.; Quaile, M. P.; Monk, J.K.; French, B.; Cappola, T. P.; Margulies, K. B. Differential expression of PDE5 in failing and nonfailing human myocardium. *Circ.: Heart Failure* **2012**, *5*, 79-86.

(10) Menniti, F.; Faraci, S.; Schmidt, C. Phosphodiesterases in the CNS: targets for drug development. *Nat. Rev. Drug Discovery* **2006**, *5*, 660-670.

(11) Puzzo, D.; Sapienza, S.; Arancio, O.; Palmeri A. Role of phosphodiesterase 5 in synaptic plasticity and memory. *Neuropsychiatr. Dis. Treat.* **2008**, *2*, 371-387.

(12) Prickaerts, J.; Sik, A.; Van Staveren, W. C.; Koopmans, G.; Steinbush, H. W.; Van der Staay, F.J.; de Vente, J.; Blokland, A. Phosphodiesterase type 5 inhibition improves early memory consolidation of object information. *Neurochem. Int.* **2004**, *45*, 915-928.

(13) Buckley, M. S.; Staib, R. L.; Wicks, L. M.; Feldman, J. P. Phosphodiesterase-5 inhibitors in management of pulmonary hypertension: Safety, tolerability, and efficacy. *Drug, Healthcare Patient Saf*. **2010**, *2*, 151-161.

(14) Giovannoni, M. P.; Vergelli, C.; Graziano, A.; Dal Piaz, V. PDE5 inhibitors and their applications. *Curr. Med. Chem*. **2010**, *17*, 2564-2587.

(15) Crom, K. F.; Curran, M. P.; Abman, S. H.; Channick, R. N.; Heresi, G. A.; Rubin, L. J.; Torbicki, A. Sildenafil: A Review of its Use in Pulmonary Arterial Hypertension. *Drugs* **2008**, *68*, 383-397.

(16) Takimoto, E.; Champion, H. C.; Li, M.; Belardi, D.; Ren, S.; Rodriguez, E. R.; Bedja, D.; Gabrielson, K. L.; Wang, Y.; Kass, D. A. Chronic inhibition of cyclic GMP phosphodiesterase 5A prevents and reverses cardiac hypertrophy. *Nat. Med.* **2005**, *11*, 214-222

(17) Salloum, F. N.; Ockaili, R. A.; Wittkamp, M.; Marwaha, V. R.; Kukreja, R. C. Vardenafil: a novel type 5 phosphodiesterase inhibitor reduces myocardial infarct size following ischemia/reperfusion injury via opening of mitochondrial KATP channels in rabbits. *J. Mol. Cell. Cardiol.* **2006**, *40*, 405-411.

(18) Szabo, G.; Radovits, T.; Veres, G.; Krieger, N.; Loganathan, S.; Sandner, P.; Karck, M. Vardenafil protects against myocardial and endothelial injuries after cardiopulmonary bypass. *Eur. J. Cardiothorac. Surg.* **2009**, *36*, 657-664.

(19) Hassan, M. A. H.; Ketat, A. F. Sildenafil citrate increases myocardial cGMP content in rat heart, decreases its hypertrophic response to isoproterenol and decreases myocardial leak of creatine kinase and troponin T. *BMC Pharmacol.* **2005**, *15*, 6-10.

(20) Guazzi, M.; Vicenzi, M.; Area, R.; Guazzi, M. D. PDE5 inhibition with sildenafil improves left ventricular diastolic function, cardiac geometry, and clinical status in patients with stable systolic heart failure: results of a 1-year, prospective, randomized, placebo-controlled study. *Circ.: Heart Failure* **2010**, *1*, 8-17.

(21) Lewis, G. D.; Shah, R.; Shahzad, K.; Camuso, J. M.; Pappagianopoulos, P. P.; Hung, J.; Tawakol, A.; Gerszten, R. E.; Systrom, D. M.; Bloch, K. D.; Semigran, M. J. Sildenafil improves exercise capacity and quality of life in patients with systolic heart failure and secondary pulmonary hypertension. *Circulation* **2007**, *116*, 1555-1562.

(22) Menniti, F. S.; Ren, J. M.; Coskran, T. M.; Liu, J.; Morton, D.; Siestsma, D. K.; Som, A.; Stephenson, D. T.; Tate, B. A.; Finklestein, S. P. Phosphodiesterase 5A inhibitors improve functional recovery after stroke in rats: optimized dosing regimen with implication for mechanism. *J. Pharmacol. Exp. Ther.* **2009**, *3*, 842-850.

(23) Menniti, F. S.; Ren, J. M.; Sietsma, D. K.; Som, A.; Nelson, F. R.; Stephenson, D. T.; Tate, B. A.; Finklestein, S. P. A non-brain penetrant PDE5A inhibitor improves functional recovery after stroke in rats. *Restor. Neurol. Neurosci.* **2012**, *4*, 283-289.

(24) Andres, J. I.; De Angelis, M.; Alcazar, J.; Celen, S.; Bormans, G. Recent advances in positron emission tomography (PET) radiotracers for imaging phosphodiesterases. *Curr. Top. Med. Chem.* **2012**, *12*, 1224-1236.

(25) Jakobsen, S.; Kodahl, G. M.; Olsen, A. K.; Cumming, P. Synthesis, radiolabelling and in vivo evaluation of [$^{11}$C]RAL-01, a potential phosphodiesterase 5 radioligand. *Nucl. Med. Biol.* **2006**, *33*, 593-597.

(26) Chekol, R.; Gheysens, O.; Cleynhens, J.; Pokreisz, P.; Vanhoof, G.; Ahamed, M.; Janssens, S.; Verbruggen, A.; Bormans, G. Evaluation of PET radioligands for in vivo visualization of phosphodiesterase 5 (PDE5). *Nucl. Med. Biol.* **2014**, *41*, 155-162.

(27) Hughes, R. O.; Rogier, D. J.; Jacobsen, E. J.; Walker, J. K.; Macinnes, A.; Bond, B.R.; Zhang, L. L.; Yu, Y.; Zheng, Y.; Rumsey, J. M.; Walgren, J. L.; Curtiss, S. W.; Fobian, Y. M.; Heasley, S. E.; Cubbage, J. W.; Moon, J. B.; Brown, D. L.; Acker, B. A.; Maddux, T. M.; Tollefson, M. B.; Mischke, B. V.; Owen, D. R.; Freskos, J. N.; Molyneaux, J. M.; Benson, A. G.; Blevis-Bal, R. M. Design, synthesis, and biological evaluation of 3-[4-(2-hydroxyethyl)piperazin-1-yl]-7-(6-methoxypyridin-3-yl)-1-(2-propoxyethyl)pyrido[3,4-b]pyrazin-2(1H)-one, a potent, orally active, brain penetrant inhibitor of phosphodiesterase 5 (PDE5). *J. Med. Chem.* **2010**, *6*, 2656-2660.

(28) Loev, B.; Musser, J. H.; Brown, R. E.; Jones, H.; Kahen, R.; Huang, F. C.; Khandwala, A.; Sonnino-Goldman, P.; Leibowitz, M. J. 1,2,4-Triazolo[4,3-a]quinoxaline-1,4-diones as antiallergic agents. *J. Med. Chem.* **1985**, *3*, 363-366.

(29) Yoshida, Y.; Sakakura, Y.; Aso, S.; Okada, N.; Okada, S.; Tanabe, Y. Practical and efficient methods for sulfonylafion of alcohols using Ts(Ms)CI / $Et_3N$ and catalytic $Me_3N$.HCI as combined base: Promising alternative to traditional pyridine. *Tetrahedron* **1999**, *55*, 2183-2192.

(30) Lakics, V.; Karran, E. H.; Boess, F. G. Quantitative comparison of phosphodiesterase mRNA distribution in human brain and peripheral tissues. *Neuropharmacology* **2010**, *59*, 367-374.

(31) Corbin, J. D.; Beasley, A.; Blount, M. A.; Francis, S. H. High level PDE5: A strong basis for treating pulmonary hypertension with PDE5 inhibitors. *Biochem. Biophys. Res. Commun.* **2005**, *334*, 930-938.

(32) Daugan, A.; Grondin, P.; Ruault, C.; Le Monnier de Gouville, A. C.; Coste, H.; Linget, J. M.; Kirilovsky, J.; Hyafil, F.; Labaudinière, R. The discovery of tadalafil: A novel and highly selective PDE5 inhibitor. 2: 2,3,6,7,12,12a-hexahydropyrazino[1′,2′:1,6]pyrido[3,4,-b]indole-1,4,-dione analogues. *J. Med. Chem.* **2003**, *46*, 4533-4542.

(33) Ishizaki, J.; Yokogawa, K.; Nakashima, E.; Ohkuma, S.; Ichimura, F. Uptake of basic drugs into rat lung granule fraction in vitro. *Biol. Pharm. Bull*. **1998**, *21*, 858-861.

(34) Soderling, S.; H, Beavo, J. A. Regulation of cAMP and cGMP signalling: New phosphodiesterases and new function. *Curr. Opin. Cell Biol.* **2000**, *12*, 174-179.

(35)Haning, H.; Niewohner, N.; Schenke, T.; Es-Sayed, M.; Schmidt, G.; Lampre, T.; Bischoff, E. Imidazo[5,1-f][1,2,4]triazin-4(3H)-ones, a new class of potent PDE 5 inhibitors. *Bioorg. Med. Chem. Lett.* **2002**, *12*, 865-868.

(36) Essayan, D. M. Cyclic nucleotide phosphodiesterases. *J. Allergy Clin. Immunol.* **2001**, *108*, 671-680.

(37) Beavo, J. A.; Rogers, N. L.; Crofford, O. B.; Hardman, J. G.; Sutherland, E. W.; Newman, E. V. Effects of xanthine derivatives on lipolysis, and on adenosine 3',5'-monophosphate phosphodiesterase activity. *Mol. Pharmacol.* **1970**, *6*, 597-603.

## Tables

**Table 1.** $IC_{50}$ (nM) values of PDE5 inhibitors for selected PDE families[a]

| Compounds | hPDE5A3 | hPDE6AB | hPDE11A4 |
|---|---|---|---|
| **10** | 16 | ND | ND |
| **10**[b] | 3.28 | 167.28 | 8068 |
| **12** | 6.60 | 3170 | 2100 |
| **14** | 1.95 | 1600 | 800 |
| **14**[b] | 0.20 | 31.60 | 492 |
| **17** | 6.45 | ND | ND |
| **18**[b] | 0.22 | 43.56 | 1082.40 |

[a]*$IC_{50}$ values are averages of duplicates;* [b]*reported $IC_{50}$ values for selected PDEs without subtype specification (Hughes et al*[27]*); ND: Not determined.*

**Table 2**. Radiochemical yield, purity and specific activty, logD and PSA values of [$^{11}$C]-**12** and [$^{18}$F]-**17.**

| Radioligand | RCY (%) | Purity (%) | [a]SA | [b]logD | [c]PSA |
|---|---|---|---|---|---|
| [$^{11}$C]-**12** | 20±13 (N = 11) | > 99 | 67 | 1.29 | 85.6 |
| [$^{18}$F]-**17** | 31±2 (N = 4) | > 99 | 91 | 1.69 | 85.6 |

*Purity determined by RP-HPLC; [a]SA (specific activity in gigabecquerel per micromole; GBq/µmol), [b]logD at pH 7.4 generated with MarvinSketch 5.5.0.1 software (ChemAxon Ltd), [c]PSA (polar surface area in Å$^2$) is software generated (Molinspiration Cheminformatics, 2011).*

# Figures

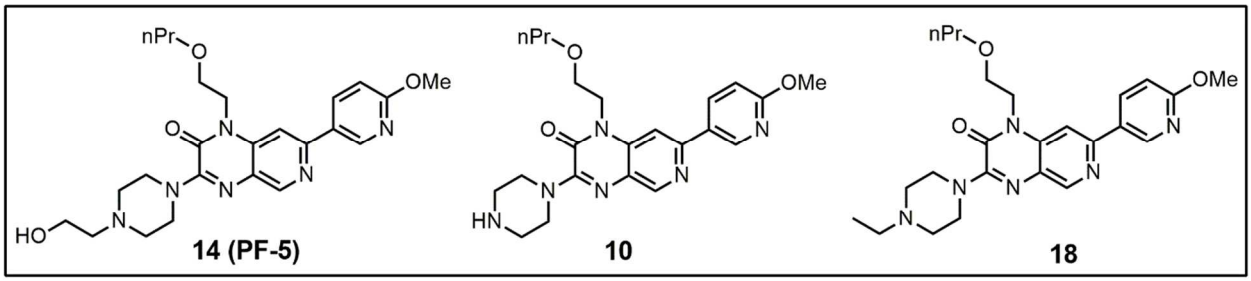


***Figure 1***. *Structure of PDE5 inhibitors* ***PF-5*** *and derivatives* ***10*** *and* ***18***[27]

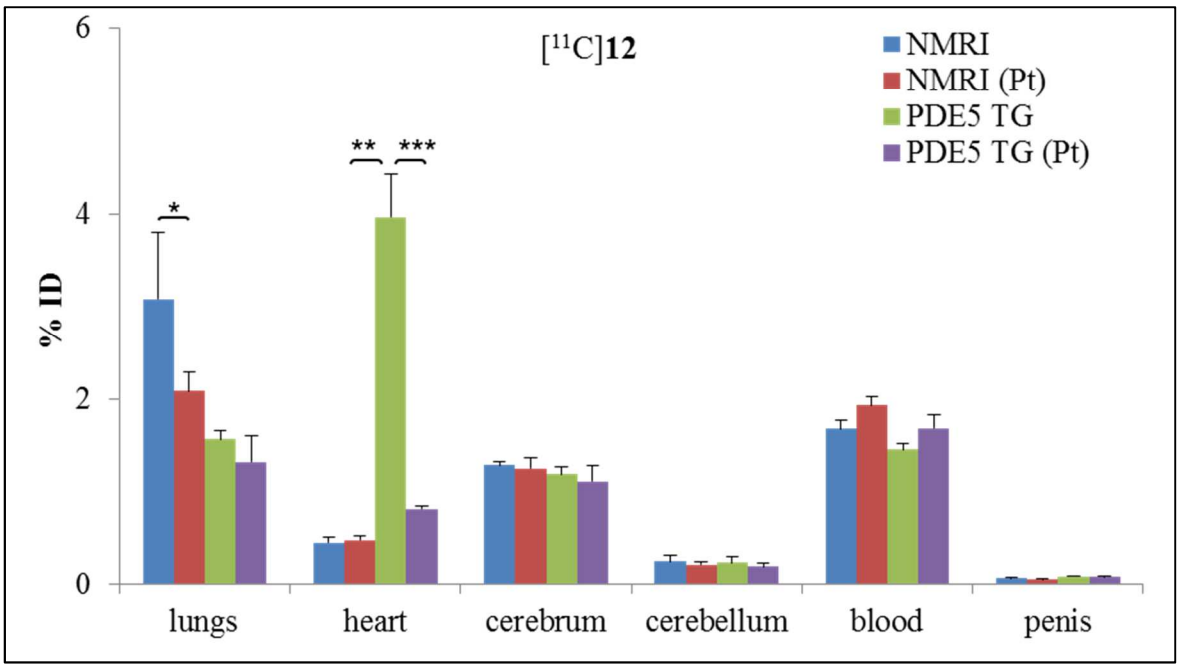


***Figure 2***. *Biodistribution results of [$^{11}$C]-**12** in NMRI wild-type mice (NMRI, N = 4), pre-treated NMRI mice [NMRI (Pt), N = 4], PDE5 TG mice (N = 4) and pre-treated PDE5 TG mice [PDE5 TG (Pt), N = 4] at 30 min pi. Pre-treatment with tadalafil, 10 mg/kg, subcutaneously, 60 min prior to tracer administration. % ID: percentage injected dose. *(p < 0.01); **(p < 0.001); ***(p < 0.0001). PDE5 TG: transgenic mice with cardiomyocyte specific over-expression of PDE5*

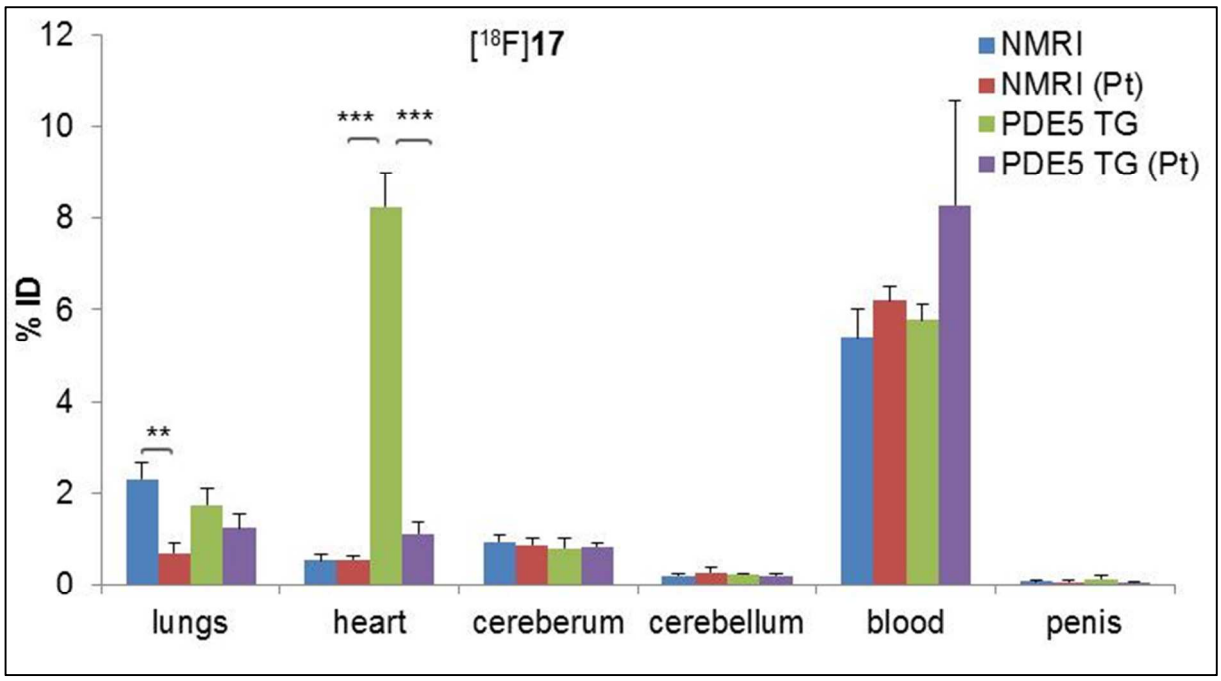


***Figure 3***. *Biodistribution results of [$^{18}$F]-**17** in NMRI wild-type mice (NMRI, N = 4), pre-treated [NMRI (Pt), N = 4)], PDE5 TG mice (N = 4) and pre-blocking [PDE5 TG (Pt), N = 4] at 30 min pi. Pre-treatment with tadalafil, 10 mg/kg, subcutaneously, 60 min prior to tracer administration. % ID: percent injected dose. **($p < 0.001$); ***($p < 0.0001$).*

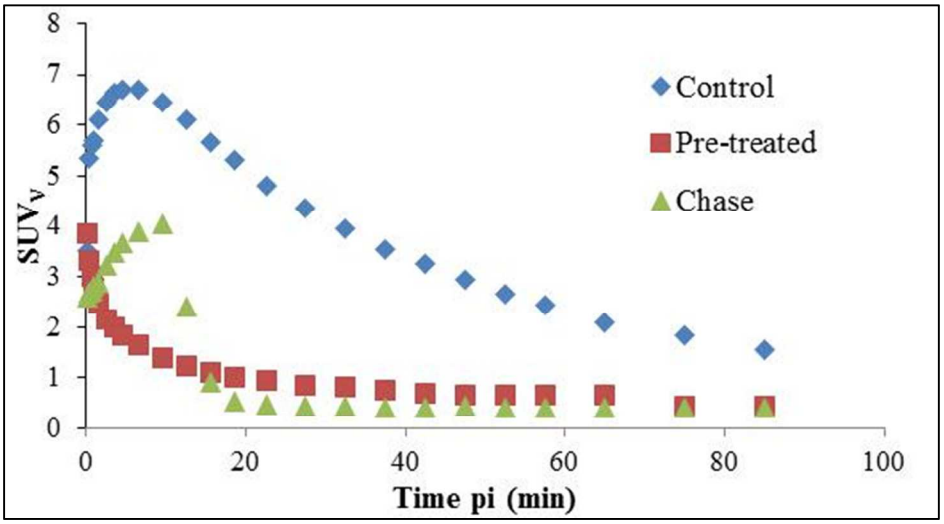


***Figure 4.*** *Myocardial time-activity-curves after intravenous injection of [$^{18}$F]-**17** (7 MBq) in PDE5 TG mice (control); PDE5 TG mice pre-treated with tadalafil (10 mg/kg, subcutaneously, 60 min prior to tracer administration) `and PDE5 TG mice chased with tadalafil (10 mg/kg, intravenously, 10 min post tracer injection). SUV$_V$: standardized uptake value based on volumetric concentration.*

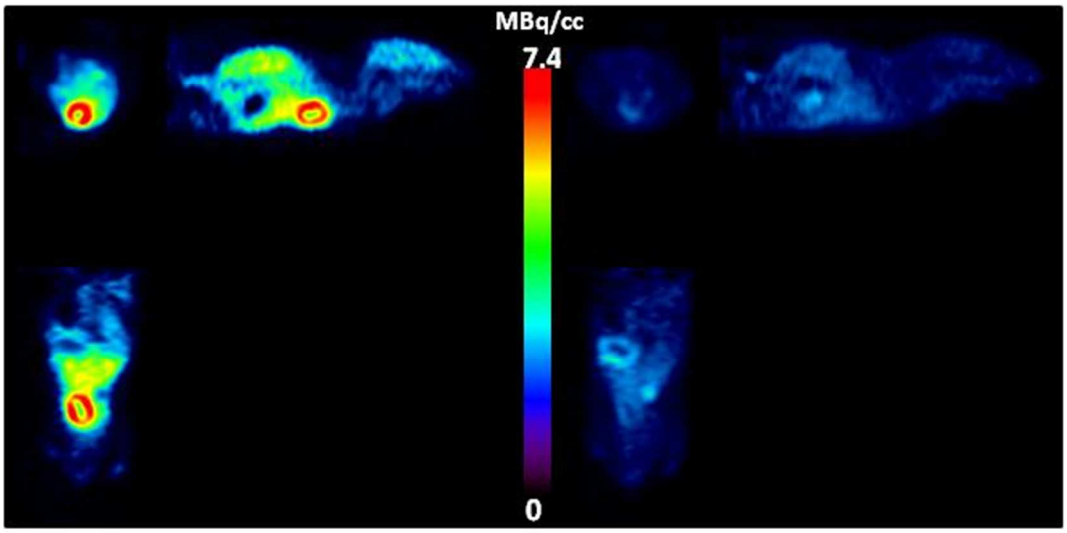


***Figure 5***. *Representative microPET images of PDE5 TG mice after injection of [$^{18}$F]-**17** (7 MBq): Left: A static reconstruction from 0 to 660s of a 90 min dynamic microPET acquisition. Right: A static reconstruction from 840 to 1500 s of the same 90 min dynamic microPET acquisition after intravenous administration of tadalafil (chase experiment)*

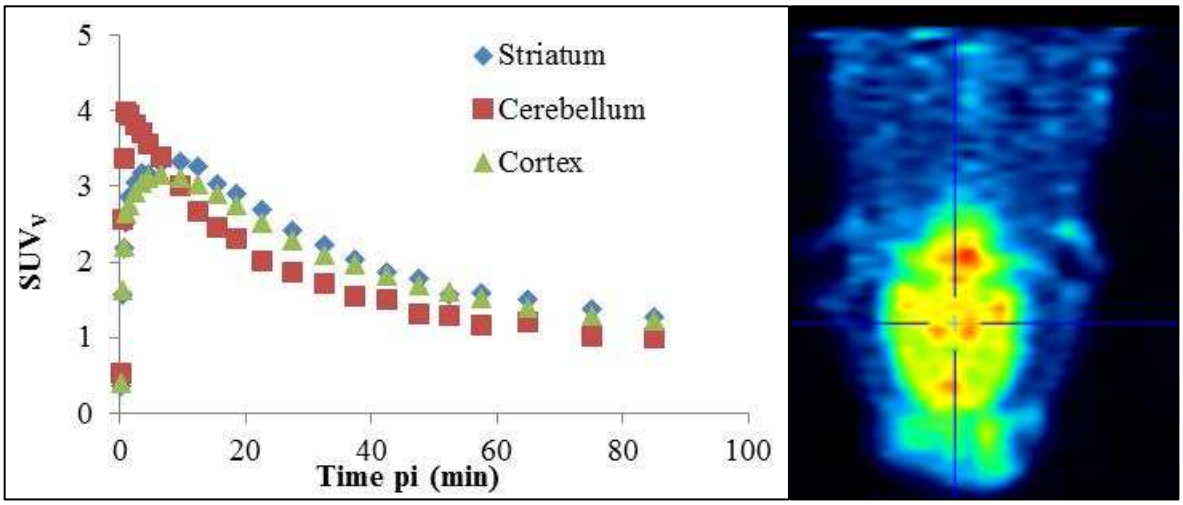


***Figure 6.*** *Left: Time activity curves of different brain regions after intravenous injection of [$^{11}$C]-**12** (37 MBq) in Wistar rats (N = 2). Right: Representative image of the brain after intravenous injection of [$^{11}$C]-**12**.*

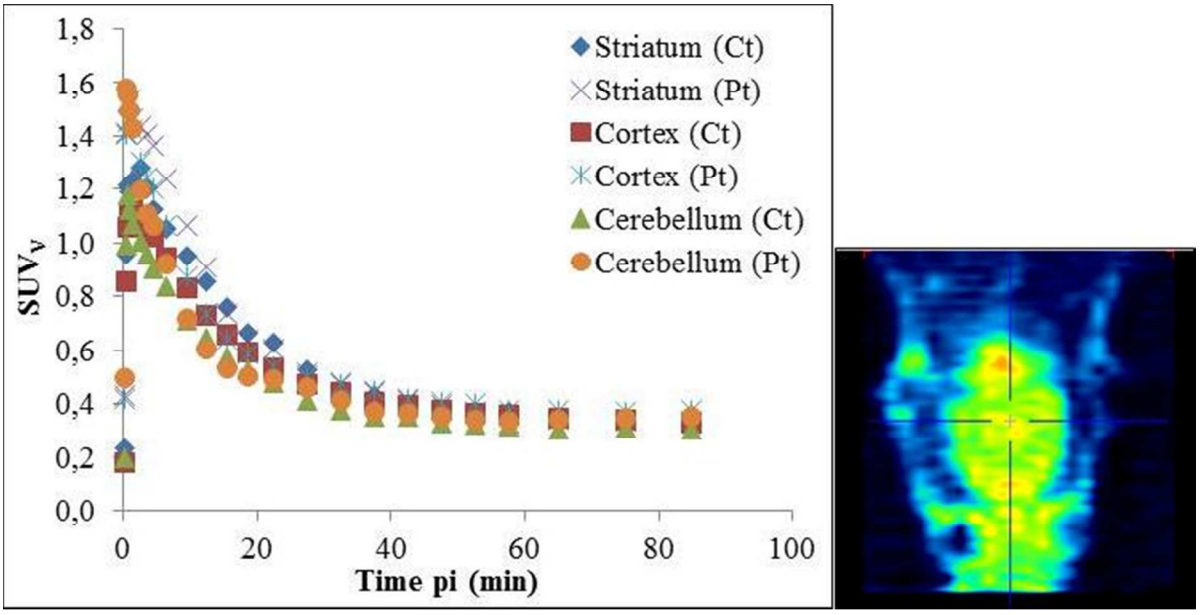


***Figure 7**. Left: Time activity curves of different brain regions after intravenous injection of [$^{18}$F]-**17** (37 MBq) in Wistar rats (N = 3); Ct: Control; Pt: Pre-treated (**17**, 10 mg/kg, subcutaneously, 60 min prior to tracer administration). Right: Representative image of the brain of a control rat after intravenous injection of [$^{18}$F]-**17** alone.*

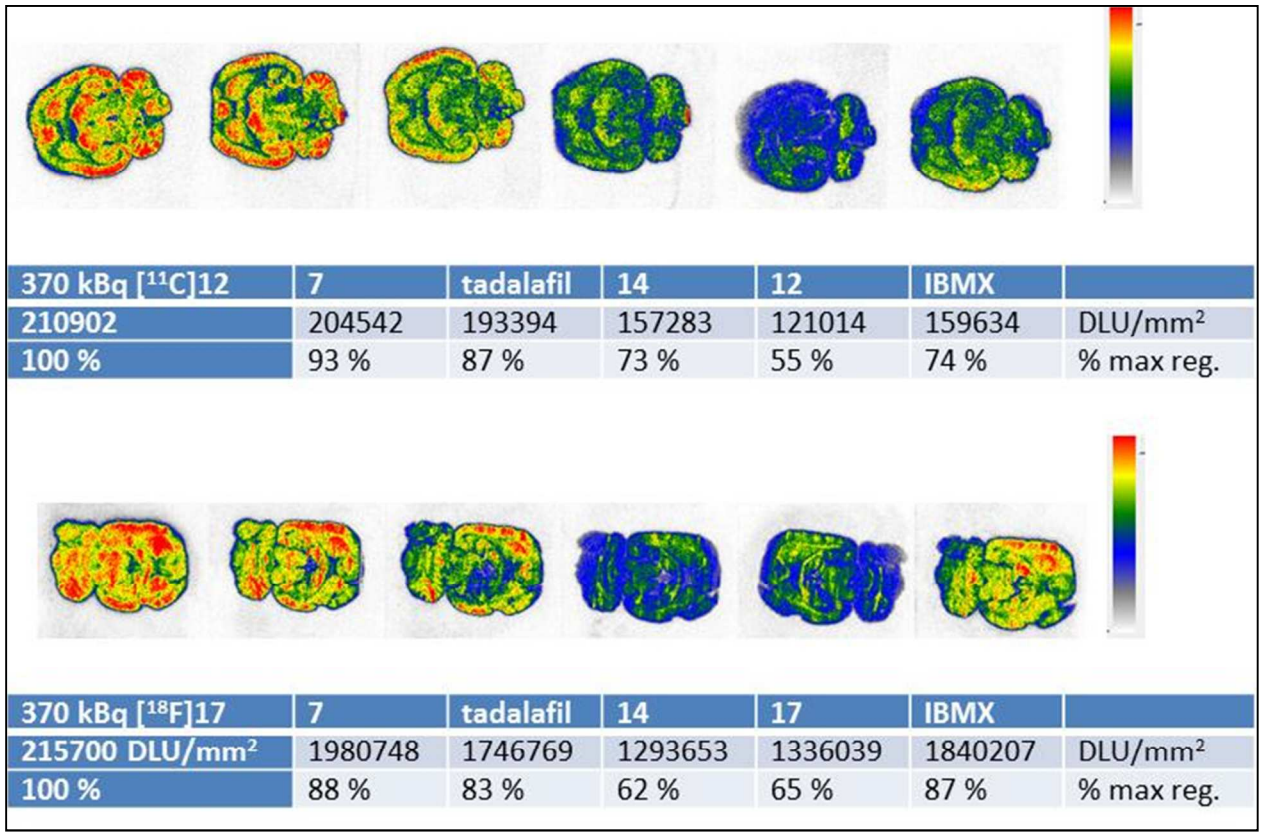

| 370 kBq [$^{11}$C]12 | 7 | tadalafil | 14 | 12 | IBMX | |
|---|---|---|---|---|---|---|
| 210902 | 204542 | 193394 | 157283 | 121014 | 159634 | DLU/mm$^2$ |
| 100 % | 93 % | 87 % | 73 % | 55 % | 74 % | % max reg. |

| 370 kBq [$^{18}$F]17 | 7 | tadalafil | 14 | 17 | IBMX | |
|---|---|---|---|---|---|---|
| 215700 DLU/mm$^2$ | 1980748 | 1746769 | 1293653 | 1336039 | 1840207 | DLU/mm$^2$ |
| 100 % | 88 % | 83 % | 62 % | 65 % | 87 % | % max reg. |

***Figure 8***. *Autoradiogram of rat brain slices incubated with [$^{11}$C]-**12** (top) and [$^{18}$F]-**17** (bottom) in the presence of different PDE inhibitors; DLU: Digital light unit; % max reg.: activity as percentage of maximum region (tracer only incubated slice as 100 % in both cases).*

**7 (NMVardenafil) = a vardenafil analogue developed by our group with in vitro PDE5 activity ($IC_{50}$) of 0.8 nM[26]. IBMX is a non-selective phosphodiesterase inhibitor.[34-37]*

## *Schemes*

**Scheme 1a.** Synthesis of lead component **7**

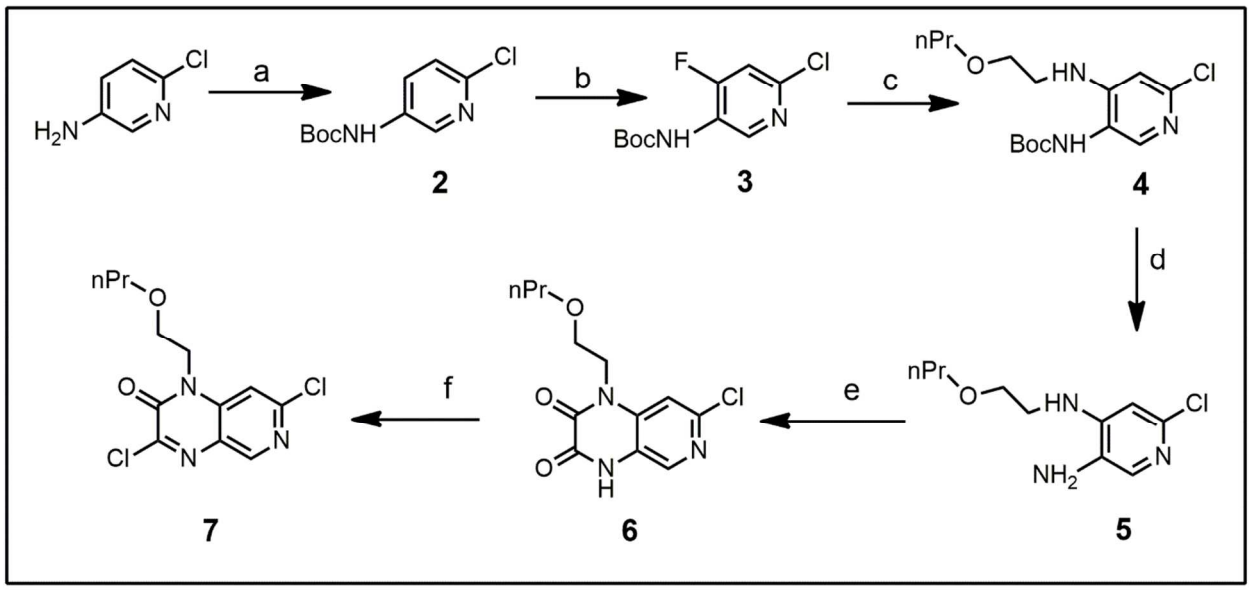

**Scheme 1b**. Synthesis of precursor and reference of [$^{11}$C]-12

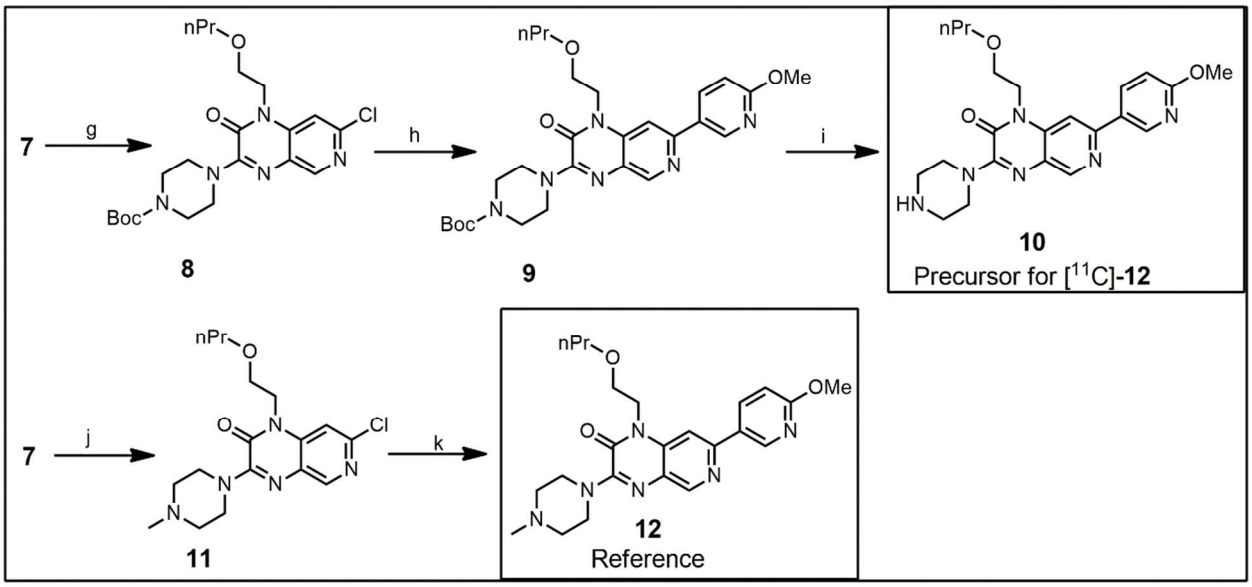

**Scheme 1c**. Synthesis of precursor and reference of [$^{18}$F]-**17**

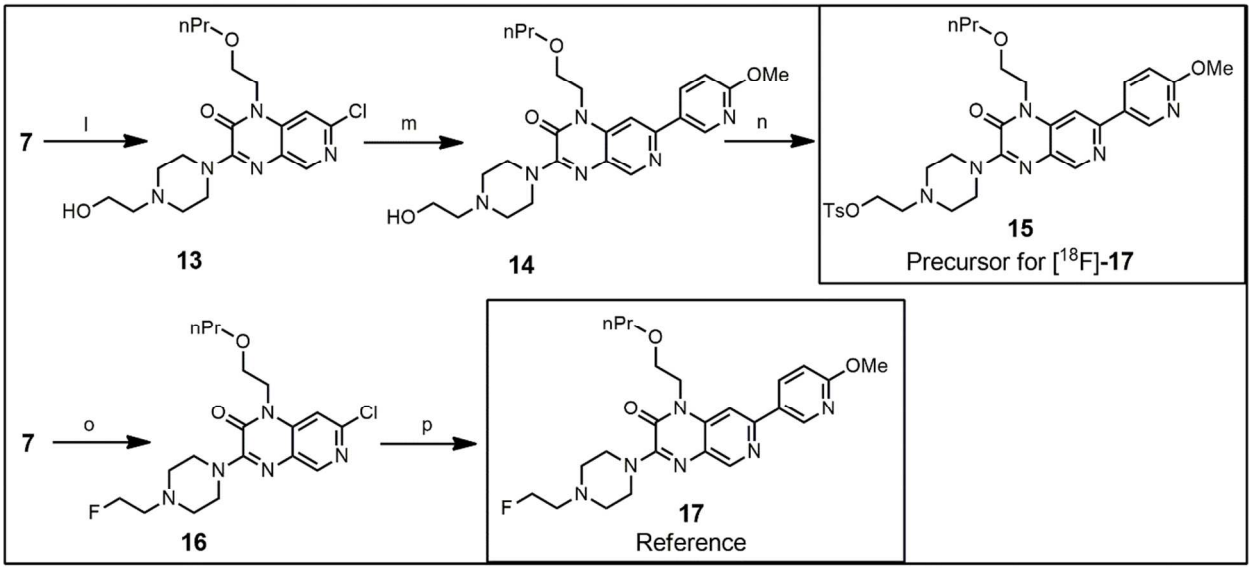

*Reagents and conditions (schemes 1a, 1b and 1c): (a) 1,4-dioxane, $(Boc)_2O$, 27 h, reflux; (b) TMEDA, n-BuLi, $Et_2O$,-60 → -10 °C, 2 h; then N-fluorobenzenesulfonimide (NFSI), THF -60 → 0 °C, 1 h, 58 %; (c) 2-propoxyethanamine, EtOH, reflux, 22 h, 70 %; (d) 4 M HCl, 1,4-dioxane, rt, 16 h, 87 %; (e) MeOC(O)C(O)Cl, i-$Pr_2NEt$, $CH_2Cl_2$, 0 °C → rt, 4 h; then PhMe, 105 °C; (f) PhMe, $SOCl_2$, DMF, 130 °C, 59 % (for steps e and f); (g) tert-butyl piperazine-1-carboxylate, $Et_3N$, THF, rt, 4 h, 83 %; (h) 6-methoxypyridin-3-ylboronic acid, $(Ph_3P)_4Pd$ (0), $Na_2CO_3$, 1,4-dioxane-EtOH, reflux, 16 h, 61 %; (i) TFA, $CH_2Cl_2$, 0 °C → rt, 16 h, 60 %; (j) same as (g) except 1-methylpiperazine, 78 %; (k) same as (h), 65 %; (l) same as (g) except 1-(2-hydroxyethyl)piperazine, 71 %; (m) same as (h), 59 %; (n) $(Et)_3N$, $(Me)_3N.HCl$, $CH_2Cl_2$, 4-methylbenzene-1-sulfonyl chloride, 0 °C → rt, 16 h, 38 %; (o) same as (g) except 1-(2-fluoroethyl)piperazine, 69 %; (p) same as (h), 50 %.*

**Scheme 2**. Radiolabeling of [$^{11}$C]-**12** and [$^{18}$F]-**17**.

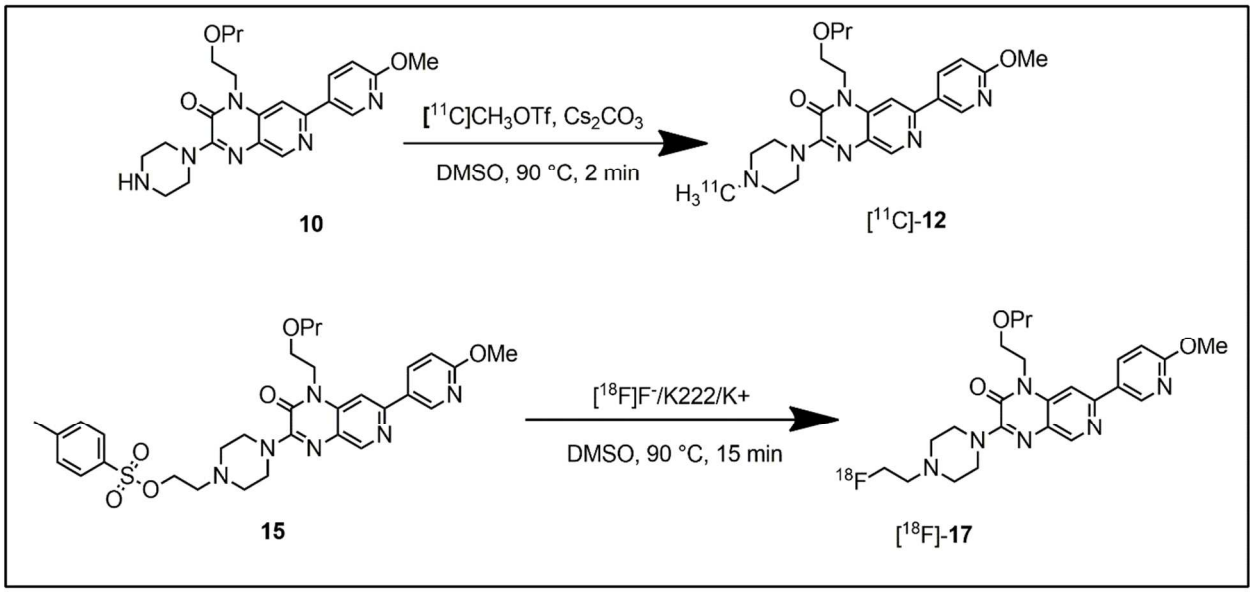

## Table of Contents graphic